Prediction of the feasibility of oriented diamond films by microwave plasma-assisted CVD

S. Barrat, E. Bauer-Grosse

Prediction of the feasibility of oriented diamond films by microwave plasma-assisted CVD

S. BARRAT, E. BAUER-GROSSE

Laboratoire de Science et Génie des Surfaces

Ecole des Mines, Parc de Saurupt 54042 NANCY Cedex (FRANCE)

Abstract

After the nucleation step, the textured or heteroepitaxial diamond film elaboration strongly depends on the direction of the fastest growth (vector denoted $_{v\ max}$) that is associated with every diamond particle. From the quantification of this vector for single-crystal and multiply twinned particles (MTPs), we can provide for the relative feasibility of textured or heteroepitaxial films in relation to the variations of elaboration conditions such as hydrocarbon concentration or substrate temperature. This theoretical study, that takes account of the results of morphological and structural characterizations of textured diamond films, reveals the difficulty to elaborate <111> textured films that lead to <011> textured films, and the easiness to obtain a <001> textured films.

1. Introduction

In the case of CVD diamond film formation on single-crystal silicon substrates, two main ways become apparent to minimize the presence of the structural faults : the elaboration of textured diamond films where the formation of a fibre axis normal to the substrate is essentially controlled by the competitive growth of randomly oriented crystals [1-5], and the elaboration of heteroepitaxial films where we promote an epitaxial relation between the diamond crystals and the silicon substrate via a β-SiC silicon carbide coating [6-9]. In both cases, the growth parameter $\alpha = \sqrt{3}.(v_{100}/v_{111})$ defined by Wild et al.[3] that fixes the growth rate ratio of the {100} and {111} single-crystal faces, is a key parameter concerning the diamond films feasibility. In the case of textured films, many studies show that their global morphology (parameter which defines both the fibre axis and the film topography) mainly depends on α. This one is related itself to the elaboration conditions, and particularly the substrate temperature and the hydrocarbon concentration [3,4]. In the same way, a recent study [5] reveals that the growth parameter choice indirectly determines the heteroepitaxial film feasibility.

From the quantification of the fastest growth $_{v\,max}$ of the single-crystals [4,5], and its extension to the MTPs, we paid particular attention to predict the feasibility of the oriented films in relation to the fibre axis stability according to a variation of the growth parameter α. Morphological and structural characterizations of textured diamond films, elaborated by a microwave plasma assisted chemical vapour deposition (MPCVD) technique [4], allows us to provide for α variations of which the consequences are in agreement with the theoretical predictions.

2. Experimental approach

2.1. Experimental step

The textured diamond films were carried out in a MPCVD reactor where the description and the synthesis conditions were detailed previously [4,10]. In order to elaborate textured diamond films with {111}{100}<111>, {111}{100}<011>, and {100}{111}<001> global morphologies, and according to the morphometric study [4], the elaboration conditions were chosen in order to fix the growth parameter at the values $\alpha^p \approx 1.14$, $\alpha^p \approx 1.50$ and $\alpha^p \approx 2.17$ respectively. The lower and upper values of α^p correspond to the limiting synthesis conditions beyond which we can observe a crystalline deterioration, or a homogeneous loss of the microwave plasma. The value

$\alpha^p \approx 1.50$ corresponds to the standard elaboration conditions that are easy to maintain and often reported in the literature.

2.2. Results

Morphological characterizations by scanning electron microscopy (figure 1) show that three types of global morphologies {111}{100}<111>, {111}{100}<011> and {100}{111}<001> are obtained for coating thickness up to 10 μm. The different elaborations reveal that the two last global morphologies are quite easy to prepare, and that the dispersion of polar orientation of crystals constituting the surface is weak (figures 1A and 1B). On the contrary, the global morphology {111}{100}<111> requires very stable elaboration conditions during the synthesis, and a high temperature deposition. The topography of this film (figure 1C) indicates a larger dispersion of the polar orientation of the crystals constituting the diamond surface. The precise experimental determination of the growth parameter α^f (f for film) by X-ray diffraction, reveals

that α^f is always higher than α^p [4]. This increase is about 0.5 but can vary according to the elaboration conditions and the substrate-holder/substrate configuration.

2.3. Discussion

We have attributed the growth parameter increase to two physical phenomena, that take place at the coalescence. This one can be associated on the one hand, to a rise of the active carbonaceous species concentration in the plasma discharge with respect to the diamond phase (figure 2A), and on the other hand, to a decrease in substrate temperature (figure 2B). Although the precise nature of the active carbonaceous species is not known, we can think that their concentrations, denoted $[C_{active}]$, is proportional to the methane concentration and consequently can modify the growth parameter. The coalescence step likely occurs with a $[C_{active}]$ increase on the substrate surface. Before the coalescence, $[C_{active}]$ permits the diamond particles to grow according to the crystal faces exposed to the plasma, and participates likewise to the silicon substrate carburization. After the coalescence, the substrate is not exposed to the plasma any more (carburization end), and the diamond surface exposed to the plasma decreases (three-dimensional to unidimensional transition). Thus, the quantity of active carbonaceous species per diamond surface unit increases and brings about a growth parameter rise. Similarly, the α increase can be due to a temperature decrease when the coalescence process occurs (figure 2B). Before the coalescence, the heat flow Q generated by the plasma discharge is dissipated by the substrate through the substrate-holder/substrate interface. Next, the diamond film formation that occurs on the whole surface of the substrate exposed to the plasma, allows the heat flow to be laterally dissipated. The additional dissipation is probably very effective taking into account the excellent thermal conductivity of diamond, and owing to the direct contact formation between the diamond film and the substrate-holder. We can also note the diamond film formation on the lower substrate face, that improves the substrate-holder/substrate contact.

The cumulative effects of the active carbonaceous species increase and the substrate temperature decrease, provoke a consequent α rise when the coalescence step occurs. At the end of the synthesis, this increase results to a α^f value higher than the α^p parameter.

3. Theoretical approach

3.1. Introduction

As reported previously [3-5], the fibre axis formation of a thick diamond film is the consequence of the competitive growth of randomly oriented crystals on the surface substrate. This fibre axis corresponds to the fastest growth $_{v\,max}$ associated with the particles constituting the diamond film. The texture of the films will be in relation to the particle shape described by α, and to the nature of these particles (single-crystals or MTPs). In the next paragraph, we shall indirectly define the $_{v\,max}$ by quantifying the disorientation angle ϕ^{th}_{hkl} as the angle between $_{v\,max}$ and the nearest crystallographic direction <hkl> for every above-mentioned particles.

3.2. Quantification and stability of the $_{v\,max}$ vector in the case of single-crystals

3.2.1 definition of ϕ^{th}_{hkl}

The $_{v\,max}$ vector, which can be described by the three indices <u v w>, and which corresponds to the largest single-crystal diameter, can take a simple form when the α^p (p for particle) domain variation is divided in two parts [5] : for $1 \leq \alpha^p \leq 1.5$, $_{v\,max}$ = <u 1 1> with $u = (3-2\alpha^p)/\alpha^p$, and for $1.5 \leq \alpha^p \leq 3$, $_{v\,max}$ = <0 v 1> with $v = (3-\alpha^p)/\alpha^p$. From these relations and the definition of the disorientation angle ϕ^{th}_{hkl}, we can plot the evolution of the three theoretical disorientations ϕ^{th}_{001}, ϕ^{th}_{011} and ϕ^{th}_{111} as a function of α^p (figure 3A). The ϕ^{th}_{hkl} variations are in agreement with the morphological evolution of the particle : for $\alpha^p = 1$, $\phi^{th}_{111} = 0$ and the particle is in cubical-shaped. For $\alpha^p = 1.5$, $\phi^{th}_{011} = 0$ and the particle is a perfect cubo-octahedron. Finally, for $\alpha^p = 3$, $\phi^{th}_{001} = 0$ and the particle is in octahedral-shaped. For instance, the figures 4A and 4B illustrate the angular disorientation ϕ^{th}_{011} relative to the <011> axis for two cubo-octahedrons that each one belongs to a defined growth parameter domain.

3.2.2. Definition of $\Delta\phi^{th}_{hkl}$

One of the main characteristic of the previous evolutions, is the slope variation $(d\phi^{th}_{hkl}/d\alpha)$ for each of the three angular disorientations ϕ^{th}_{hkl}, that vary according to the α^p domain. Since the three theoretical slopes have the same evolution with α^p, and since the <011> axis is the common direction to the two growth parameter domains, we have chosen to study the $\Delta\phi^{th}_{011}$ variation that is illustrated figure 3B. We have plotted the evolution of this angular disorientation dispersion as a function of α^p when this one is lightly modified

($\Delta\alpha = \pm 0.01$). On the whole, $\Delta\phi_{011}^{th}$ decreases when α^p rises. We noted that $\Delta\phi_{011}^{th}$, which indirectly quantifies the $_{v\,max}$ stability in relation with a small α^p variation, is more important for the α value near 1. This instability strongly decreases when α^p draws near to 1.50. Finally, for the α^p values near 3, the $_{v\,max}$ instability is weak and evolves little. These tendencies can be interpreted as a large morphological dispersion of the single-crystals when their shapes are near the cube ($\alpha^p < 1.5$). On the contrary, the elaboration of single-crystals near octahedron results in a weak morphological dispersion.

3.3. Case of multiply twinned particles

As reported previously [4], there is a significative proportion of MTPs such as icosahedrons or Wulff decahedrons, where $_{v\,max}$ does not systematically agree with the vector associated with the single-crystals previously studied. Nevertheless, it is possible to define this vector for the main cases $\alpha^p = 1$, $\alpha^p = 1.5$ or $\alpha^p = 3$. In the case of the icosahedron, $_{v\,max}$ corresponds to the <111> direction for $\alpha^p = 1$, and the <011> direction for $\alpha^p > 1.5$. In the case of the Wulff decahedron, morphometric analysis reveals that for a small α^p value, the particle extends by its pseudo-fivefold axis. For a larger value of α^p, the decahedral particle is rather "star-like". If we associated $_{v\,max}$ to the largest particle diameter, this vector corresponds to the <001> direction for the high values of α^p. It corresponds to the <011> direction for smaller α^p values ($\alpha^p \leq 1.5$). In some cases, the direction of fastest growth associated with the MTPs corresponds to the direction of fastest growth of single-crystals (this is the case of the icosahedron for $1 \leq \alpha^p \leq 1.5$, and the Wulff decahedron for $1.5 \leq \alpha^p \leq 3$). In the other complementary domains, $_{v\,max}$ of single-crystals and MTPs differ.

3.4. Consequences on the fibre axis of oriented films

$\Delta\phi_{011}^{th}$ that quantifies the $_{v\,max}$ stability, quantifies also the feasibility of the <u v w> texture, that is itself determined by the α^p value. Thus, for α^p near 1 where the global morphology is {111}{100}<111>, the resulting <111> texture is relatively unstable since a small α^p variation (± 0.01) provokes an angular variation of $_{v\,max}$ more important than for a <001> texture. This tendency is particularly visible when α^p draws near to 1.5. A little additional increase in α^p rapidly induces a {100}{111}<011> global morphology which is more stable. On the contrary, for a film with a growth parameter near 3, the <001> fibre axis is relatively stable with regard to a small α variation. Thus, in the case of the near <111> textured film elaboration, local

variations of the growth parameter infer a global morphology dispersion, i.e. a proportion of the crystals on the surface which have not the orientation imposed by the elaboration conditions. This dispersion will be the less important as the growth parameter will be near 3. In some cases, the presence of MTPs can perturb the formation of the desired global morphology if the correspondent $_{v\,max}$ vector does not agree with the desired texture. This will be the case for a small α^p (texture <111>) where the Wulff decahedron has a <011> fastest growth, and for a high α^p (texture <001>) where the icosahedron has a <011> fastest growth.

4. Discussion

The theoretical and experimental approaches lead to think that the global morphology formation essentially depends on the growth parameter α^p, and its evolution during the diamond film growth. Experiments show that α^p systematically increases when the film formation occurs [4]. This rising, whose direction is illustrated figure 3B, facilitates the <001> texture formation in the domain $1.5 \leq \alpha^p \leq 3$, but limits the formation of the {111}{100}<111> global morphology in the domain $1 \leq \alpha^p \leq 1.5$. This difficulty is strengthened by a strong instability of the <111> texture, that leads to form a <011> texture in the case of growth parameter variations. These ones do not significantly influence the <001> textured films where $\Delta\phi^{th}_{011}$ varies little in the domain $1.5 \leq \alpha^p \leq 3$. These conclusions are in agreement with the previous experimental study, which reveals the difficulty to obtain the <111> texture and also their morphological dispersion (figure 1C). The presence of decahedral particles does not disturb the <001> texture formation since their correspondent $_{v\,max}$ is the <001> direction. We can think that the presence of icosahedrons disturbs this texture since their $_{v\,max}$ is the <011> direction. In fact, the experiment shows that the MTPs proportion increases with the temperature. The <001> texture formation occurring a low temperature (high α^p), the icosahedrons quantity is low and does not significantly modify the <001> texture. On the contrary, the <111> texture formation is strongly disturbed by the presence of the Wulff decahedrons with a $_{v\,max}$ equal to <011>, and whose proportion is more important for the temperature conditions where α^p is small. These tendencies are experimentally confirmed because the films with the {111}{100}<111> global morphology are difficult to obtain, and rarely reported in the literature. Concerning the heteroepitaxial film elaboration, we can foresee the same evolution because the crystal growth alike depends on the growth parameter α^p. The elaboration of <111> heteroepitaxial films will be more delicate than the <001> films according to the literature [8]. Finally, the

thickening of a heteroepitaxial film being submitted to the competitive growth of crystals whose some of them have a random orientation, it is preferable to choice $_{v\,max}$ identical to the silicon orientation in order to favour the epitaxial crystals. On the contrary, we can observe an epitaxial loss due the preferential selection of randomly oriented crystals as reported by Wild et al. [5].

5. Conclusion

The elaboration and the structural and morphological characterizations of diamond films with {111}{100}<111>, {111}{100}<011> and {100}{111}<001> global morphologies have shown that the <001> textured films elaboration is more easy than the <111> textured films. This is due to a growth parameter α increase when the film formation occurs, and a weak global morphology dispersion associated with the relative stability of the <001> texture. This increase is attributed to the cumulative effects of the active carbonaceous species increase and the substrate temperature decrease when the crystals coalescence occurs. The theoretical study of the angular disorientation variation $\Delta\phi_{hkl}^{th}$ (and specially $\Delta\phi_{011}^{th}$) as a function of α shows that the <111> textured film elaboration can produce a dispersion of the {111}{100}<111> global morphology because of the instability of the <111> texture in relation to a small growth parameter variation. This instability, associated with the natural α increase at the coalescence step, can produce a <011> textured film. This effect can be accentuated by the presence of decahedral particles whose direction of fastest growth is the <011> direction when α^p is near 1, and whose proportion increases when the substrate temperature rises. These predictions are in agreement with the morphological observations that reveal a global morphology dispersion in the case of <111> textured films. An extension of these previsions can be performed in the case of heteroepitaxial films that always contain some randomly crystals that yield to the competitive growth for the same reason as the textured films.

Acknowledgments

The authors would like to thank I. Dieguez for the diamond syntheses and the DRET for financial support.

References

[1] Ch. Wild, N. Herres, P. Koidl, *J. Appl. Phys.*, 68 (1990) 973.

[2] R.E. Clausing, L. Heatherly, L.L. Horton, E.D. Specht, G.M. Begun, Z.L. Wang *Diamond and Relat. Mater.*, 1 (1992) 411.

[3] C. Wild, P. Koidl, W. Müller-Sebert, H. Walcher, R. Kohl, N. Herres, R. Locher R. Samlenski, R. Brenn, *Diamond and Relat. Mater.*, 2 (1993) 158.

[4] S. Barrat, I. Dieguez, H. Michel, E. Bauer-Grosse *Diamond and Relat. Mater.*, 3 (1994) 520.

[5] C. Wild, R. Kohl, N. Herres, W. Müller-Sebert, P. Koidl *Diamond and Relat. Mater.*, 3 (1994) 373.

[6] B.R. Stoner, S.R. Sahaida, J.P. Bade, P. Southworth, P.J. Ellis *J. Mater. Res.*, 8 (1993) 1334.

[7] X. Jiang, C.P. Klages, R. Zachai, M. Hartweg, H.J. Füsser *Appl. Phys. Lett.*, 62 (1993) 3438.

[8] M. Schreck, R. Hessmer, S. Geier, B. Rauschenbach, B. Stritzker *Diamond and Relat. Mater.*, 3 (1994) 510.

[9] I. Dieguez, E. Bauer-Grosse, *C.R. Acad. Sci. Paris*, t.318, Série II (1994) 1607.

[10] S. Barrat, H. Michel, E. Bauer-Grosse, *Surf. Coat. Technol.*, 59 (1993) 330.

Figures

Figure 1

Scanning electron micrographs of textured diamond films elaborated at Pt = 40 hPa, deposition time 120 h, [Ar] = 25 vol.% on Si <001> :

(A) : {100}{111}<001>, T = 920 K, [H_2] = 74.4 vol.%, [CH_4] = 0.6 vol.%, α^p = 2.17

(B) : {111}{100}<011>, T = 1050 K, [H_2] = 74.4 vol.%, [CH_4] = 0.6 vol.%, α^p = 1.50

(C) : {111}{100}<111>, T = 1160 K, [H_2] = 74.8 vol.%, [CH_4] = 0.2 vol.%, α^p = 1.14

Figure 2

Schematic representation of the α increase at the coalescence step :

(A) : increase of the active carbonaceous species concentration

(B) : decrease of the substrate temperature

Figure 3

(A) : ϕ^{th}_{hkl} evolution as a function of α^p for the three <001>, <011> and <111> directions

(B) : $\Delta\phi^{th}_{011}/\Delta\alpha^p$ evolution as a function of α^p (for $\Delta\alpha^p = \pm 0.01$)

Figure 4

Definition of the disorientation angle ϕ^{th}_{011} according to the cuboctahedral shape

(A) : cuboctahedron with α^p = 1.20

(B) : cuboctahedron with α^p = 2.50

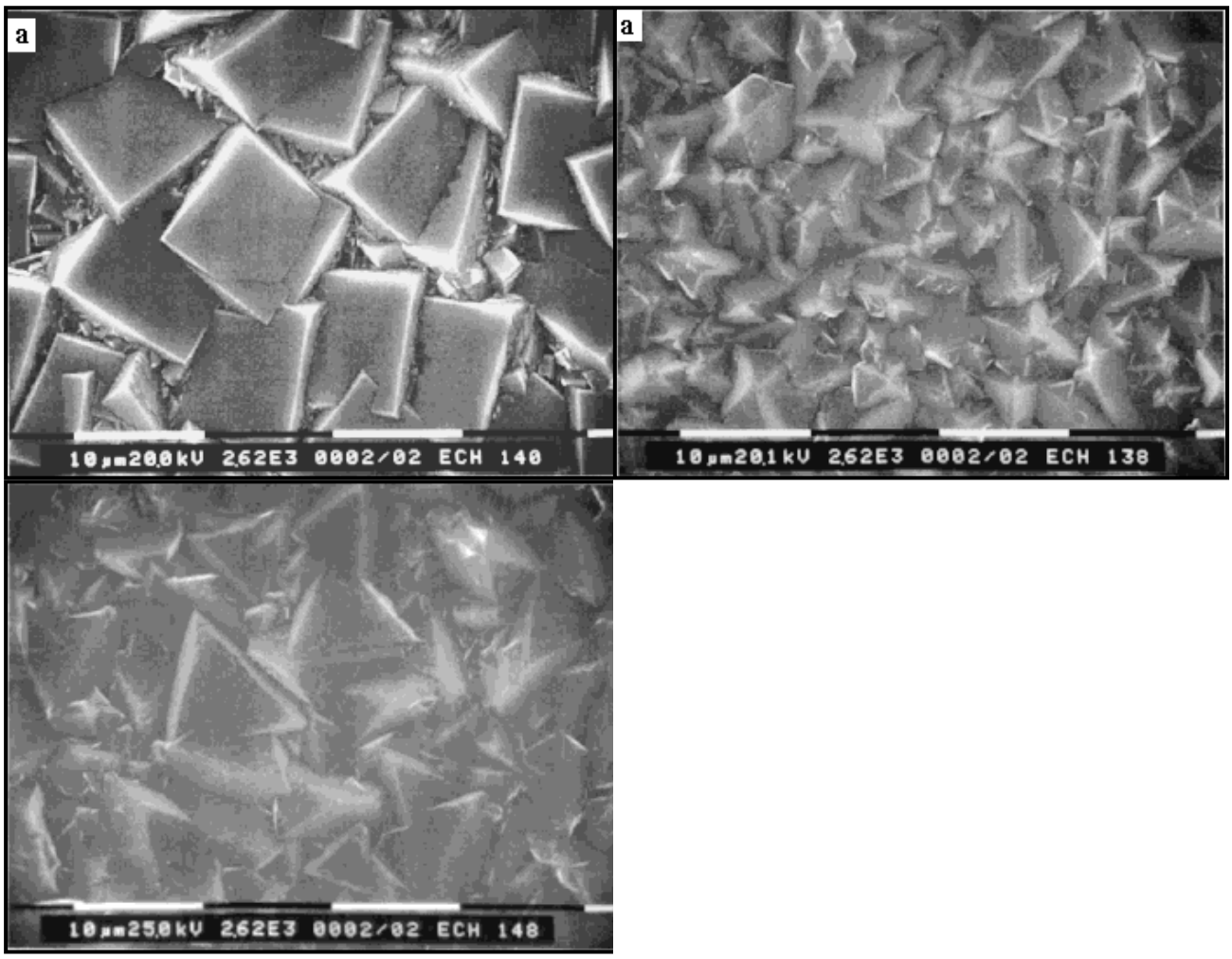
a
10µm20.0kV 2.62E3 0002/02 ECH 140
a
10µm20.1kV 2.62E3 0002/02 ECH 138
10µm25.0kV 2.62E3 0002/02 ECH 148

Figure 1

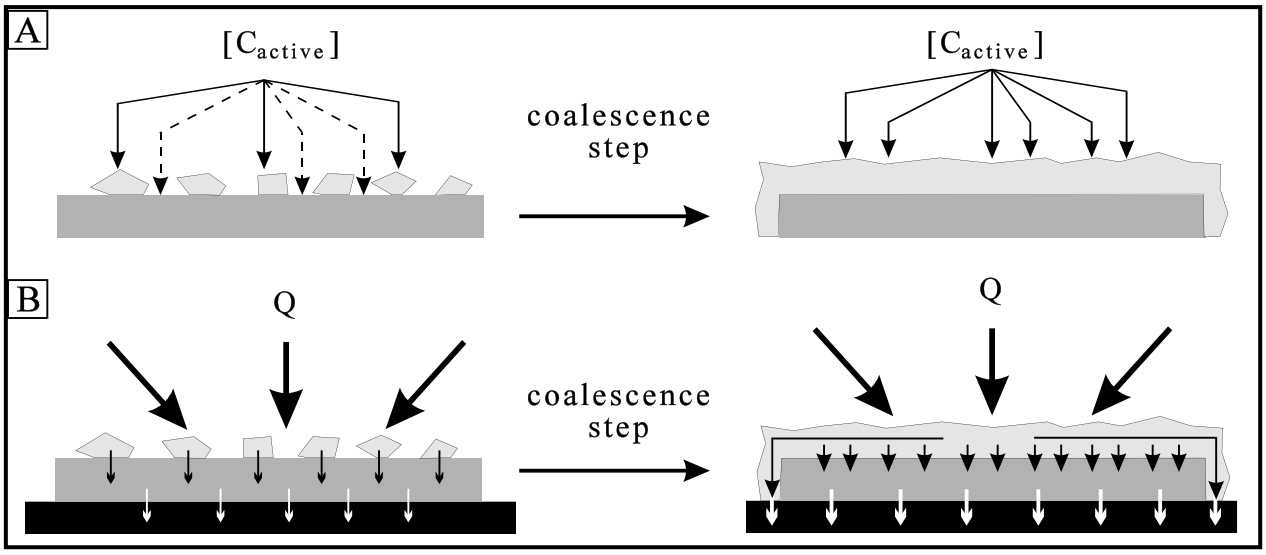

Figure 2

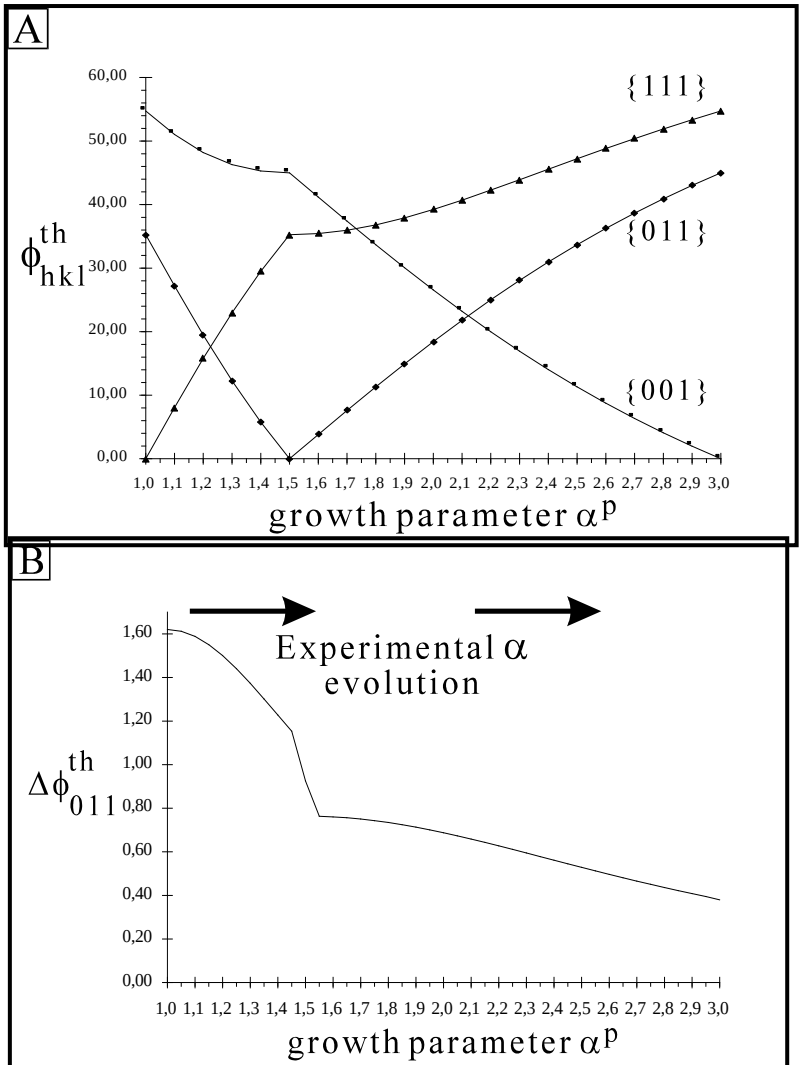
A
60,00
50,00
40,00
30,00
20,00
10,00
0,00
ϕ^{th}_{hkl}
{111}
{011}
{001}
1,0 1,1 1,2 1,3 1,4 1,5 1,6 1,7 1,8 1,9 2,0 2,1 2,2 2,3 2,4 2,5 2,6 2,7 2,8 2,9 3,0
growth parameter α^p
B
Experimental α evolution
1,60
1,40
1,20
1,00
0,80
0,60
0,40
0,20
0,00
$\Delta\phi^{th}_{011}$
1,0 1,1 1,2 1,3 1,4 1,5 1,6 1,7 1,8 1,9 2,0 2,1 2,2 2,3 2,4 2,5 2,6 2,7 2,8 2,9 3,0
growth parameter α^p

Figure 3

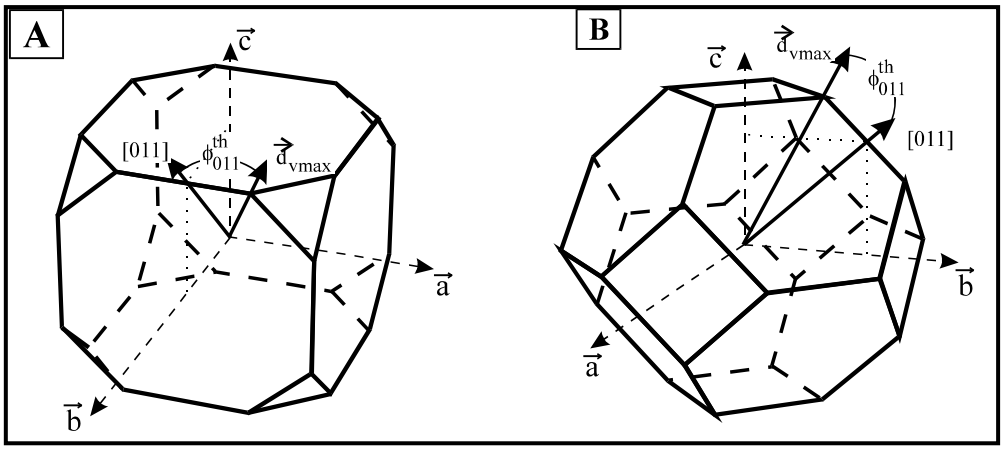
A
$\vec{c}$
[011]
ϕ^{th}_{011}
$\vec{d}_{vmax}$
$\vec{a}$
$\vec{b}$
B
$\vec{d}_{vmax}$
$\vec{c}$
ϕ^{th}_{011}
[011]
$\vec{b}$
$\vec{a}$

Figure 4